Electrochimica Acta 144 (2014) 111–118

Contents lists available at ScienceDirect

Electrochimica Acta

journal homepage: www.elsevier.com/locate/electacta

Electrochemical Detection of Nitric Oxide and Peroxynitrite Anion in Microchannels at Highly Sensitive Platinum-Black Coated Electrodes. Application to ROS and RNS Mixtures prior to Biological Investigations

Yun Li, Catherine Sella, Frédéric Lemaître, Manon Guille-Collignon, Laurent Thouin*, Christian Amatore*

Ecole Normale Supérieure-PSL Research University, Département de Chimie, Sorbonne Universités - UPMC Univ Paris 06, CNRS UMR 8640 PASTEUR, 24, rue Lhomond, 75005 Paris, France

ARTICLE INFO

Article history:
Received 16 May 2014
Received in revised form 2 August 2014
Accepted 5 August 2014
Available online 26 August 2014

Keywords:
RNS
ROS
electrochemical detection
microchannel electrode
Pt-black electrode

ABSTRACT

The electrochemical detection of nitric oxide ($NO^{\bullet}$) and peroxynitrite anion ($ONOO^-$) was investigated at Pt-black electrodes in microchannels. Owing to the high reactivity of these species under conditions close to physiological media, kinetic parameters were determined before evaluating the detection performances from synthetic solutions. Highly sensitive and stable Pt-black electrodes allowed detection limits down to 30 nM ($NO^{\bullet}$) and 40 nM ($ONOO^-$) to be reached with very high sensitivities. As $NO^{\bullet}$ and $ONOO^-$ are two relevant biological molecules involved in oxidative stress their simultaneous detections with other major molecules like hydrogen peroxide and nitrite were also performed and validated experimentally at pH 8.4. These results demonstrated that relative ROS/RNS contents in synthetic mixtures can be easily assessed at selected detection potentials. Beyond the interest of using small volumes in microfluidic channels, optimization of detection requires precise conditions easy to implement. These were delineated to lead in microdevices to high-performances detection of oxidative stress metabolites either from analytes or from the production of a few living cells like macrophages.

1. Introduction

Oxidative stress is a process involved in many physiological and pathological situations (cancers, neurodegenerative diseases, autoimmune pathologies). Over the last decades, broad researches have been devoted to the study of the different phases of this process. Recent results have demonstrated the ubiquitous imbrication in metabolism of reactive oxygen species (ROS) with that of nitric oxide (nitrogen monoxide, $NO^{\bullet}$) [1]. The exact balance between these species and products controls many cell functions. They are also meaningful risk markers in case of traumatic injuries [2]. However, the simultaneous production of superoxide and nitric oxide by living cells leads to a series of complex and interconnected pathways in oxidative stress [3]. Effects of nitric oxide in organisms depend on its local concentration but also on specific conditions prevailing in vivo [4]. Nitric oxide is a weak oxidant by itself but it reacts extremely fast with paramagnetic species. Therefore, when superoxide anion $O_2^{\bullet -}$ and $NO^{\bullet}$ are produced in a restricted cell environment, they couple at a rate close to the diffusion limit leading to the production of peroxynitrite anion $ONOO^-$ [5]. $ONOO^-$ is reported as a powerful oxidant and cytotoxic agent. It is the source of many oxidative, nitrating and nitrosating processes involving several cell components [1,6].

The challenging development of analytical methods for monitoring the production of nitric oxide and peroxynitrite is therefore highly warranted [7,8]. This is key to better understanding the role played by these species in human health care, heavy diseases and pathologies. Among existing methods, fluorescence and chemiluminescence measurements allow extracellular high performance detection of nitric oxide [9–15] and peroxynitrite [16,17]. However, in comparison, electroanalytical methods remain advantageous due to their unparalleled spatial and temporal resolutions [18]. Indeed, despite inherent difficulties, micro-electrochemistry provides powerful tools to estimate concentration levels very close to the location from which species are produced. Electroanalytical techniques are also the only ones able to determine intracellular [19] and extracellular [3,20,21] minute fluxes of ROS/RNS in real-time without disturbing the metabolism of living cells. They are label-free since nitric oxide and peroxynitrite can be detected

* Corresponding authors.
E-mail addresses: laurent.thouin@ens.fr (L. Thouin), christian.amatore@ens.fr (C. Amatore).

http://dx.doi.org/10.1016/j.electacta.2014.08.046
0013-4686/

electrochemically at specific potentials [8,22–29]. This contrasts with the poor selectivity of many redox fluorescent markers [17]. Both species oxidize at relatively low potentials [30] even if their detections are more demanding due to their short half-life under physiological conditions [22,24,26,31,32]. In some previous studies, we demonstrated that microelectrodes could be used to monitor extracellular fluxes of nitric oxide and peroxynitrite released from single activated fibroblasts [33–35] or macrophages [36–39]. Under these experimental conditions, the excellent sensitivity and temporal resolution of the measurements resulted from the very short distance separating the microelectrode surface from single cells. However, the performances of such individual measurements were in practice constrained by cellular variability. Repetitive series of measurements were thus required to obtain reliable statistical information. In this respect, microelectrodes integrated into microfluidic devices should facilitate the whole procedure if detection of extracellular fluxes of ROS and RNS is performed at once on a collection of cells gathered in a microchamber [36,40,41]. This approach would meet the two necessary requirements for detection of highly reactive species, i.e., small sample volumes and short analysis times.

Detection of ROS and RNS in microsystems remains a challenge. Under those circumstances, the pH employed, mixing dynamics and composition of the media are important [42]. Electrochemical performances are also often limited by the ensuing poisoning of metallic electrodes such as Pt electrodes [43]. Convective flow in microsystems is expected thus to minimize these inhibitions and increase at the same time the detection sensitivity. In this context, we demonstrated recently that the simultaneous electrochemical detection of hydrogen peroxide (H_2O_2) and nitrite (NO_2^-) could be performed in microfluidic channels at highly sensitive platinum-black coated platinum electrodes [44]. In the following work, we wish to report an extension of this approach to the case of the other two important reactive species, nitric oxide NO• and peroxynitrite anion $ONOO^-$. One problem here is the kinetic stability of these two species when the detection is not preformed closely above a single cell (viz., at a few μm) but in a microfluidic channel. Taking benefit of optimized Pt-black deposits, the electrochemical detections were thus studied using calibrated synthetic solutions of NO• and $ONOO^-$. In association with H_2O_2 and NO_2^-, conditions were further delineated to reach high-performances in microfluidic channels for detecting the four primary ROS and RNS in the mixtures.

2. Experimental section

2.1. Materials and solutions

Phosophate-buffered saline (PBS) was use as buffer for most experiments. PBS was prepared from tablets (Life Technologies) dissolved into pure water and composed of 10 mM Na_2HPO_4, 2.68 mM KCl and 140 mM NaCl (pH 7.4). Water was obtained from a Milli-Q purification system (resistivity 18.2 MΩ cm at 25 °C; Millipore). Peroxynitrite solutions were prepared from dilution of 40 mM alkaline sodium peroxynitrite solution (NaONOO; Cayman Chemicals) with a mixture of 0.01 M PBS and 0.1 M NaOH so as to reach the required pH, between 11.1 and 8.4. This pH was systematically controlled with a pH meter (Radiometer Analytical). Stock solutions of 50 mM DEA-NONOate [45,46] were initially prepared by dissolving 10 mg of solid DEA-NONOate (Cayman Chemicals) in 0.96 mL of 0.01 M NaOH. Solid DEA-NONOate was previously stored under nitrogen at -80 °C to avoid any decomposition. Similarly, stock solutions were stored at 0 °C after preparation for 24 h maximum before use. To initiate the release of NO•, minute volumes of a stock solution were rapidly mixed with aerated PBS buffer (pH 7.4) to provide DEA-NONOate tested solutions. Hydrogen peroxide and nitrite solutions were freshly prepared in PBS from stock solutions (H_2O_2: 35 wt%, Acros; NO_2^-:1 M from 99.99% $NaNO_2$, Aldrich) before experiments. Since peroxynitrite and DEA-NONOate solutions decompose with time, the duration t_0 between the solution preparation and beginning of experiments was recorded and reported systematically in kinetic studies.

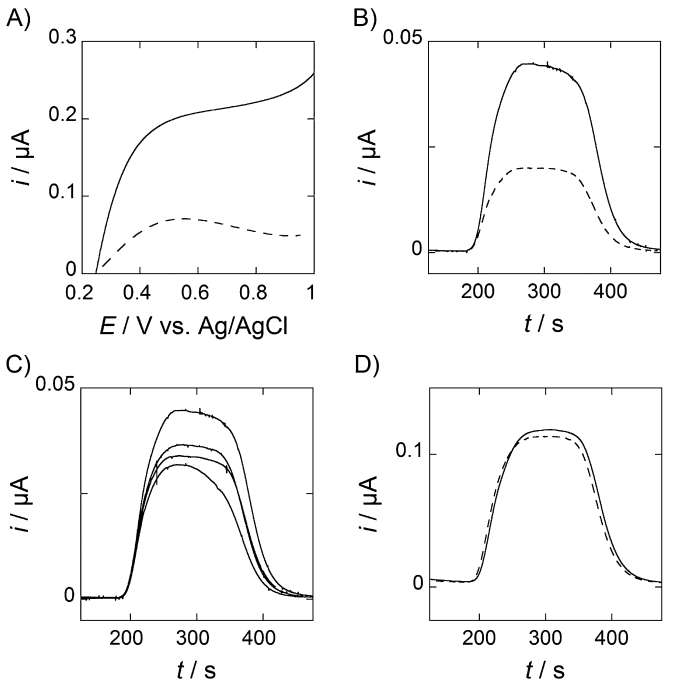

Fig. 1. (A) Voltammograms in a continuous flowing solution of 0.1 mM $ONOO^-$ at bare-Pt (dashed line) and Pt-black electrodes (solid line) at pH 11.1. (B) Current responses of $ONOO^-$ microinjections at bare-Pt electrode before (dashed line) and after (solid line) electrode activation. (C) From top to bottom, current responses of repetitive $ONOO^-$ microinjections at bare-Pt electrode after electrode activation. (D) Current responses of $ONOO^-$ microinjections at Pt-black electrode before (dashed line) and after (solid line) electrode activation. In (B-D) Microinjections of 0.1 mM $ONOO^-$ solution at pH 11.1 and E = 0.45 V/REF. x-axis refers to time after solution preparation.

Pt-black deposition solutions were prepared from 1 mL hydrogen hexachloroplatinate (IV) solution (8% wt in water; Sigma-Aldrich) and 1.6 mg lead (II) acetate trihydrate (99.8%; Sigma) added into 6.36 mL PBS. Lead ions were required as an impurity to initiate and control the Pt-black growth during electrodeposition [47].

2.2. UV-Vis spectra

Absorbance of peroxynitrite and DEA-NONOate solutions was monitored at room temperature (22 °C) using a UV-Vis spectrophotometer (Lambda 45; Perkin Elmer) at λ = 302 nm and 250 nm for peroxynitrite and DEA-NONOate solutions respectively.

2.3. Microdevices

Design and fabrication of microdevices were as reported in our previous work (see Fig. 1 in [44]). The upper layer comprised three independent parallel channels made by casting polydimethylsiloxane (PDMS, RTV-615; Momentive Performance Materials) onto a 20 μm-thick SU-8 2015 photoresist (Microchem) patterned mold. Reservoirs and injection channels were punched in the PDMS layer after it was peeled off. The under layer was a glass substrate on which several platinum microbands (working electrodes,

WEs; 197 μm width) were patterned by soft lithography and deposited (Ti/Pt with 8 nm/25 nm thickness) using a sputtering coater (K675XD; Emitech). Some WEs were further platinized upon reduction of Pt (IV) from deposition solutions at a constant current density (-8 $mAcm^{-2}$). A silver microband was partly oxidized to be used as a reference Ag/AgCl electrode (REF; 500 μm width). It was fabricated by sputtering 50 nm Ag onto the underlying Pt surface and oxidizing it by 5 mM $FeCl_3$ (Sigma). The counter electrode was a Pt electrode band (CE; 500 μm width) placed downstream the WEs. The two channel components, PDMS layer and glass substrate, were then assembled irreversibly by means of oxygen plasma (Harrick), so that the microchannels were set perpendicular to the microband electrodes (see Fig. 1 in ref [44]). REF and CE were located respectively upstream and downstream the WEs according to the flow direction. The effective lengths of all electrodes were limited by microchannel width (200 μm) and the volume of solution above the microbands was restricted by the microchannel height (20 μm). During each experiment, only one WE was connected and only one channel was filled with solution, the others remaining empty.

2.4. Electrochemical experiments

All electrochemical experiments were performed versus a home made Ag/AgCl reference electrode (REF) at room temperature using a potentiostat (Autolab PGSTAT 30; Eco Chemie) controlled by GPES 4.9 software. The flow was pressure-driven by a syringe pump (Pump 11 Elite; Harvard Apparatus) at constant average flow rate of 2 $\mu Lmin^{-1}$. According to the device geometry, it corresponded to a laminar flow regime [48]. Before some electrochemical measurements, electrodes were activated by applying a series of alternating potential pulses (+0.2 V, 1 s and -0.5 V, 1 s; 30 cycles) in flowing PBS. Analytes were introduced in microchannels in two ways, either as a continuous flow of solution or via microinjections of solution in a continuous PBS flow through a peek sample loop (5 μL; Rheodyne) to mimic oxidative bursts. In the first case, voltammograms were recorded at a scan rate of 10 mVs^{-1}. In both cases, chronoamperometric measurements were performed in order to monitor current variations during the passage of analytes above electrodes or to monitor current decay with time for kinetic evaluations. Calibration curves were established from microinjections with various sample concentrations down to 0.1 μM. Detection limits (LOD) were calculated from independent tests (at least 10 tests) with samples in the nanomolar concentration range. For this evaluation, three times the standard deviation of the measurements and calibration slope were considered.

2.5. Theoretical simulations

The differential equation associated to the kinetic of $NO^{\bullet}$ release (see Eq. (9)) was solved using COMSOL Multiphysics 4.2 software. A mathematical model based on least squares analysis of experimental kinetics was used to ensure optimal fit between experimental and calculated data. This model took into account predictions resulting from previous simulations of mass transport regimes at channel microband electrodes [48].

3. Results and discussion

3.1. Peroxynitrite detection

Since peroxynitrite decomposes rather rapidly at physiological pH, we had to take into account its chemical stability during the following electrochemical investigation. The evaluation of the kinetics was thus a necessary step before assessing the performances of electrochemical detection achieved in microchannels. Since the pK of peroxynitrous acid (ONOOH) is about 6.8 [5,49,50], both the acid and anion are present at physiological pH. However, the acid is unstable and rearranges into nitrate:

$$ONOOH \rightarrow NO_3^- + H^+ \quad (1)$$

At higher pH, a decomposition pathway prevails with the production of dioxygen and nitrite:

$$ONOOH + ONOO^- \xrightarrow{k} O_2 + 2NO_2^- + H^+ \quad (2)$$

This reaction proceeds via the formation of peroxynitric acid as intermediate during the following sequence [24]:

$$ONOOH + ONOO^- \rightarrow NO_2^- + O_2NOO^- + H^+ \rightarrow 2NO_2^- + O_2 + H^+ \quad (3)$$

However, in most cases of interest here, the overall decomposition of $ONOO^-$ in Eq. (2) is first order and decreases upon increasing pH [51]. At physiological pH, the decay becomes more complex and depends on the nature of the buffer [52]. The half-life time of $ONOO^-$ is estimated about 1 s. This makes the $ONOO^-$ detection particularly challenging for the analysis of its production by living cells or its content in biological samples. Note that under other circumstances, $ONOO^-$ can also react rapidly with carbonyls [53] and metals [54].

The electrochemical oxidation of $ONOO^-$ is a one-electron reaction, whatever the pH [30]:

$$ONOO^- \rightarrow ONOO^{\bullet} + e^- \quad (4)$$

Conversely, $ONOO^-$ is sufficiently stable in alkaline conditions with an acceptable extended lifetime [24,32,50] (e.g., 5 hours in 0.3 M NaOH at 25 °C). We then performed electrochemical experiments at pH 11.1. Indeed, it was previously demonstrated that the oxidation wave of $ONOO^-$ was independent of pH down to 8.5 [30]. This allows the electrochemical properties of $ONOO^-$ to be evaluated from more stable solutions [7,30]. Note that these conditions do not ensure at this stage any reliability of measurements in biological environments. Higher pH than 11.1 were avoided to prevent degradation of Pt-black electrodes. Measurements were carried out at bare-Pt and Pt-black electrodes fabricated according to the procedure described in experimental section. Fig. 1A compares voltammograms obtained in case of a continuous solution flow of $ONOO^-$ at bare-Pt and Pt-black electrodes. In each case peroxynitrite started to be oxidized at potentials higher than 0.2 V/REF. At Pt-black electrodes a steady-state diffusion mass transport regime was reached above 0.45 V/REF as evidenced by a limiting current (or current plateau) at high potentials. In contrast, a peak-shaped voltammogram was observed under same conditions at bare-Pt electrodes of same surface areas with current intensities two times lower. This behavior demonstrated that oxidation of $ONOO^-$ on bare-Pt was altered by a more complex pathway involving other limiting steps and by some competitive poisoning of Pt surface. This was confirmed by performing $ONOO^-$ detection at a constant potential of 0.45 V/REF after several injections of $ONOO^-$ solutions (Fig. 1B-D). Activation of electrodes, prior to detection, led to a noticeable increase of current at bare-Pt electrodes (Fig. 1B). In this case, a flow-removal of residues adsorbed on Pt surface as well as a selective activation of Pt sites led to an enhancement of the electrochemical oxidation. However, intensities reached after activation still remained lower than those recorded at Pt-black electrodes. Note also that the measurement repeatability was not satisfactory since current responses for successive $ONOO^-$ microinjections decreased with time from one to the other (Fig. 1C). On the contrary, currents recorded at Pt-black electrodes were more stable and no significant change was observed of current level before and after activation (Fig. 1D). Such electrode treatment led to more reproducible results with higher long-term performances as it was

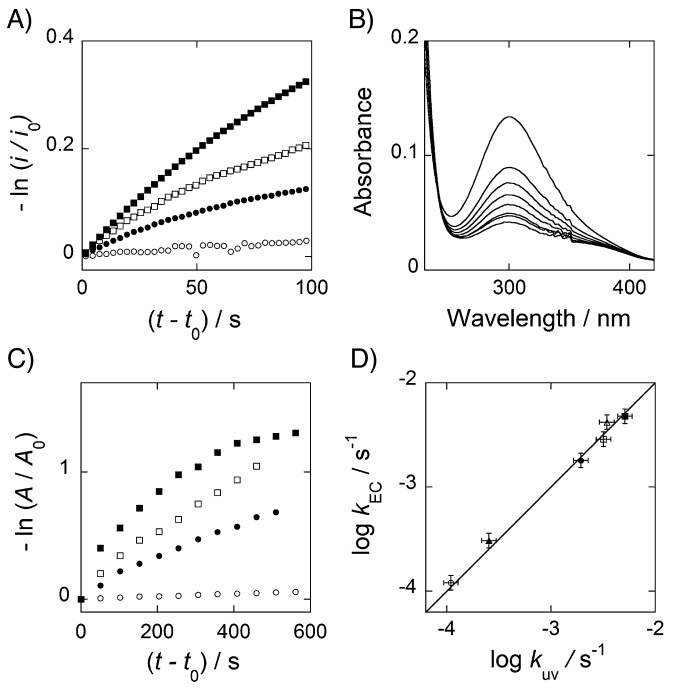

Fig. 2. (A) Current intensities monitored at Pt-black electrode in 0.1 mM $ONOO^-$ continuous flowing solutions at several pH. E = 0.45 V/REF and t_0 = 130 s. (B) Repetitive UV-Vis spectra starting from 20 s after solution preparation with 51 s time intervals of 0.1 mM $ONOO^-$ solution at pH 8.4. Absorbance decreases with time. (C) Variations of UV-Vis peak intensities at several pH of 0.1 mM $ONOO^-$ solution at λ = 302 nm, t_0 = 40 s. (D) Comparison between kinetic constants evaluated from electrochemical detection (k_{EC}) and UV-Vis spectra analysis (k_{UV}) at times lower than 200 s after solution preparation. In (A,D) pH = 11.1 (open circle), 10.8 (solid triangle), 10.2 (solid circle), 9.4 (open square), 8.9 (open triangle) and 8.4 (solid square).

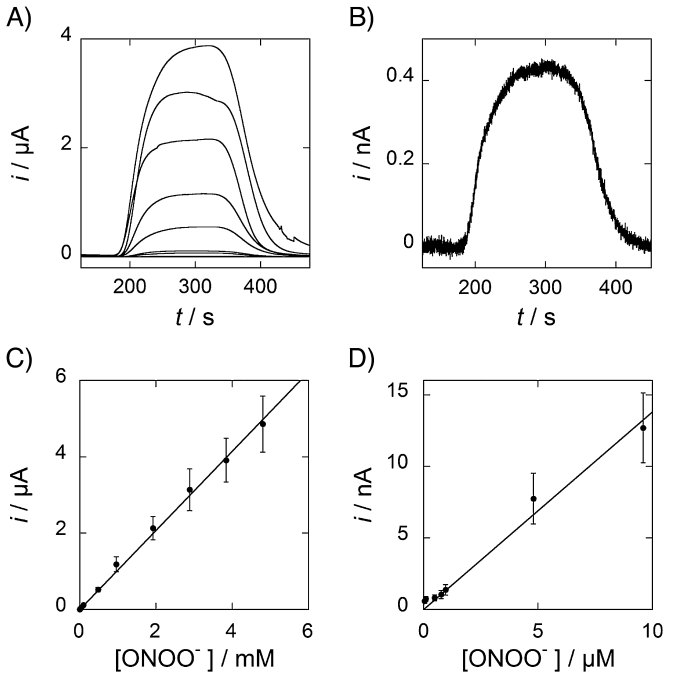

Fig. 3. (A) Current responses at Pt-black electrode of $ONOO^-$ microinjections with various concentrations. From top to bottom: 4, 3, 2, 1, 0.5 and 0.1 mM, 50, 10, 5, 1, 0.5 and 0.1 µM. x-axis refers to time elapsed after solution preparation. (B) Current response of 50 nM $ONOO^-$ microinjection. (C-D) Calibration curves of $ONOO^-$ detection at Pt-black electrode. Currents monitored 300 s after solution preparation and concentrations evaluated for $k = 1.2\ 10^{-4}\ s^{-1}$. Linear curve fit with slope equal to $1.04\ 10^{-3}$ AM^{-1}. In (A-D) pH = 11.1 and E = 0.45 V/REF.

confirmed in case of tests performed with a large number of electrodes (data not shown). From an electroanalytical point of view, $ONOO^-$ detection was by far more efficient on optimized Pt-black electrodes than on bare-Pt electrodes.

These first results were confirmed by investigating the kinetics of $ONOO^-$ decomposition at lower pH. Electrochemical measurements were achieved at Pt-black electrodes and compared to those obtained under the same conditions from UV-Vis spectra (Fig. 2). In both cases $ONOO^-$ decomposition was found to be first order over a range of 200 s after the solution preparation (Fig. 2A and C). At higher times, the kinetic profile was more complex as significant deviations from linear logarithmic plots occurred when pH tended to 8.4. This trend was consistent with other mechanisms proposed under similar conditions [5]. The evaluation of the first-order kinetic constant k (Eq. (2)) from both types of measurements led to very similar results (Fig. 2D). Accordingly, k increased by almost two orders of magnitude from 10^{-4} to $10^{-2.5}$ s^{-1} when pH decreased from 11.1 to 8.4. All these data were also in very good agreement with other values reported in the literature [5,30,32,50].

These results demonstrated the feasibility and reliability of $ONOO^-$ detection at Pt-black electrodes. Calibration curves were established from injections of different $ONOO^-$ solutions at pH 11.1 (Fig. 3A). For that purpose, a wide range of concentrations was investigated after correcting them by taking into account the kinetics of $ONOO^-$ decomposition at this pH. $ONOO^-$ concentrations were estimated after the time delay separating the measurements from the solution preparation. Values on current plateau were also subtracted from residual currents monitored in the absence of $ONOO^-$. Calibration curves thus obtained displayed linear relationships with four decades linearity and a sensitivity of 2.64 $AM^{-1}cm^{-2}$ (Fig. 3C-D). Conversely, linearity was no longer observed at concentration below 100 nM (Fig. 3D). The limit of detection (LOD) assessed from calibration slope and repetitive measurements in low concentration range was 40 nM. This limit agreed with data reported elsewhere [7,32,55]. However, this limit reflected other limitations than signal-to-noise ratio since currents reached at 50 nM were still far larger than noise (Fig. 3B). Note that such LOD does not relate to expected concentrations in biological systems. It applies to any extracellular concentrations emitted by a cells population. Their detected values depend on the experimental conditions including device geometry. Evaluation of concentrations in microfluidic channels is thus a prerequisite for the determination of amounts of species released upstream. The calibration curve allowed the diffusion coefficient of $ONOO^-$ to be estimated leading to $D_{ONOO^-} = (1.4 \pm 0.2)\ 10^{-5}\ cm^2 s^{-1}$. According to theoretical steady-state currents predicted under the hydrodynamic regime of interest in the present microchannels (*see* experimental section), this value was close to those usually considered for RNS in similar conditions [56–59].

3.2. Nitric oxide detection

The performances of NO• detection were evaluated using dynamic NO• concentrations generated through the decomposition of DEA-NONOate solutions. Preliminary studies evidenced that the decomposition rate depended strongly on the concentration of DEA-NONOate and pH. Therefore, NO• generation rates were carefully investigated through kinetic evaluations performed under the conditions used in this study. DEA-NONOate solutions chemically decompose into NO• (75% yield) when dissolved into aqueous solutions at physiological pH according to [60]:

$$Et_2N - [N(O)NO]^- Na^+ + H^+ \xrightarrow{k1} 2\,NO^\bullet + Et_2NH + Na^+ \quad (5)$$

with a rate law of DEA-NONOate global decomposition given by:

$$V_1 = k_1[Et_2N\text{-}[N(O)NO]^-] \quad (6)$$

where k_1 = 7.22 10^{-4} s^{-1} at 22 °C at pH 7.4 [61].

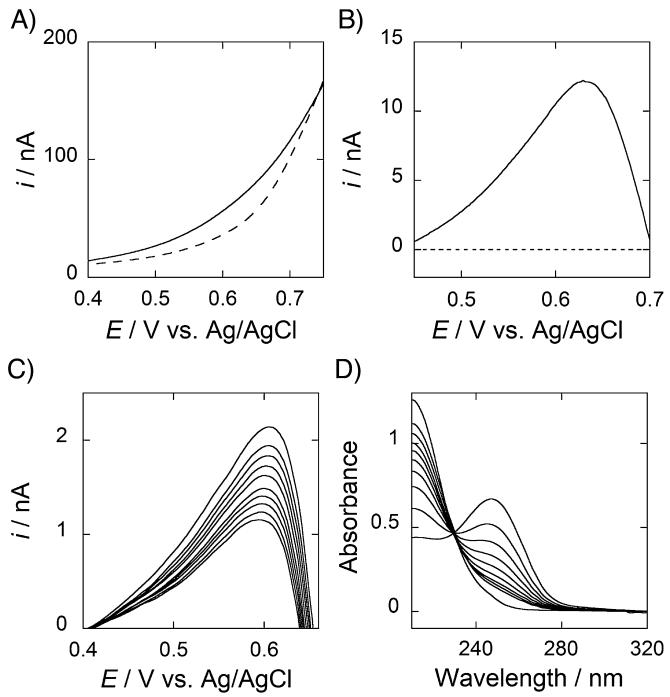

Fig. 4. (A) Voltammograms in a continuously DEA-NONOate flowing solution at Pt-black electrode. Voltammograms recorded 270 s (solid line) and 770 s (dashed line) after solution preparation. (B) Background corrected voltammograms at bare-Pt (dotted line) and Pt-black electrodes (solid line), 270 s after solution preparation. (C) Corrected voltammograms at Pt-black electrodes, 230 (top) to 730 s (bottom) after solution preparation. (D) UV-Vis spectra, 120 to 9000 s after solution preparation. In (A-B) 0.5 mM DEA-NONOate solution, pH = 7.4. In (C-D) 0.1 mM DEA-NONOate solution at pH = 7.4.

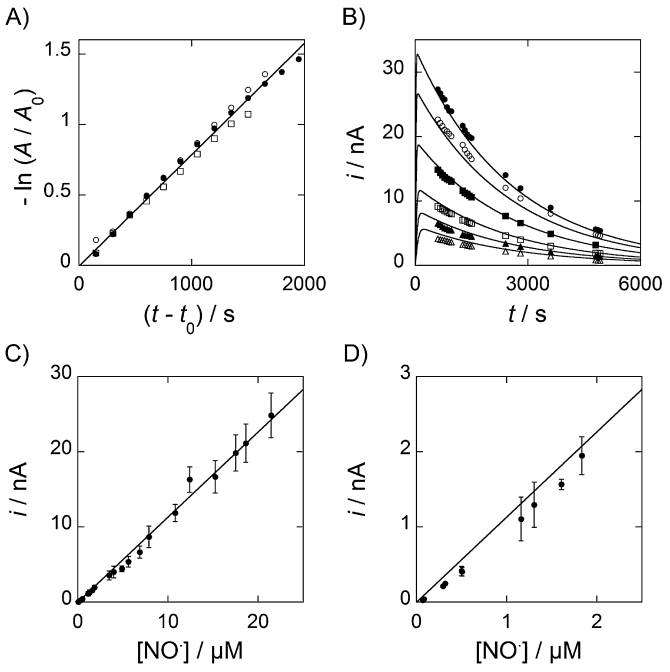

Fig. 5. (A) Analysis of UV-Vis peak intensities for three series of measurements in 0.1 mM DEA-NONOate solution at pH 7.4. t_0 = 40 s and λ = 250 nm. Linear curve fit with slope equal to $k_1 = 7.8\,10^{-4}\,s^{-1}$. (B) Theoretical (solid lines) and experimental (symbols) chronoamperometric currents at Pt-black electrodes for various concentrations of DEA-NONOate flowing solutions. From top to bottom: 1.5 (solid circle), 1 (open circle), 0.5 (solid square), 0.2 (open square), 0.1 (solid triangle) and 0.05 mM (open triangle). Curve fit with $k_1 = 7.8\,10^{-4}\,s^{-1}$, $k_2\,[O_2] = 5.5\,10^2\,M^{-2}s^{-1}$ and $i/[NO^\bullet] = 1.13\,10^{-3}\,AM^{-1}$. (C-D) Calibration curves for NO• detection at Pt-black electrode established from DEA-NONOate flowing solutions of various concentrations ranging from 1500 to 0.1 μM, at pH 7.4. Corrected currents monitored 850 and 1200 s after solution preparation. Linear curve with slope equal to $1.13\,10^{-3}\,AM^{-1}$. In (B-D) E = 0.62 V/REF and pH = 7.4.

However, NO• concentration results from the competition between the fast DEA-NONOate decomposition (Eq. (5)) and the slower reaction of NO• with oxygen [62]:

$$4\,NO^\bullet + O_2 + 2\,H_2O \xrightarrow{k2} 4\,NO_2^- + 4H^+ \quad (7)$$

which obeys a second order rate low given by:

$$V_2 = 4k_2[NO^\bullet]^2[O_2] \quad (8)$$

where $k_2 = (2.3 \pm 0.6)\,10^6\,M^{-2}s^{-1}$ at 20-25 °C [46,62–67].

Since the efficiency of NO• release is about 75% in Eq. (5),1.5 mole of nitric oxide is generated per mole of DEA-NONOate [68]. Therefore, the kinetic profile of NO• release follows the balance between V_1 and V_2:

$$d[NO^\bullet]/dt = 1.5k_1\exp(-k_1t)[Et_2N\text{-}[N(O)NO]^-]_0 - 4k_2[NO^\bullet]^2[O_2] \quad (9)$$

where $[Et_2N\text{-}[N(O)NO]^-]_0$ is the initial concentration of DEA-NONOate. Since V_1 is much larger than V_2, NO• concentration increases faster at very short times, reaches a maximum and then decays slowly [45]. Note that the corresponding half-life time of DEA-NONOate is 16 min at 22 °C in 0.1 M phosphate buffer at physiological pH [61]. To ensure that the time-course and concentration level of produced NO• were enough to complete adequate detections, we first performed measurements not later than 20 min (i.e., 1200 s) after the solution preparation. Electrochemical detection of NO• was performed through its one-electron oxidation process according to:

$$NO^\bullet \rightarrow NO^+ + e^- \quad (10)$$

Fig. 4A shows voltammograms obtained under these conditions at Pt-black electrode at 270 and 770 s. However, extracting the electrochemical oxidation current for NO• required a correction from background currents. So, voltammograms recorded after complete NO• decomposition were subtracted from the initial response (Fig. 4B). This was a necessary step since NO• reaction with oxygen (Eq. (7)) produces nitrite anions that accumulate and start to oxidize at slightly higher potentials [44]. It is also known that NO• donors like DEA-NONOate generate potential interfering species issued from own NO• reactivity or other decomposition products [60]. After background currents subtraction a wave was obtained with a maximum at E = 0.62 V/REF in contrast to a plateau expected under steady-state regime of mass transport. This electrochemical behavior could be related to the progressive electrode poisoning by side-products of DEA-NONOate decomposition and products released during the potential scan. This was also confirmed by the progressive current amplitude decay in successive voltammograms recorded as a function of time (Fig. 4C). Nevertheless, in comparison to bare-Pt electrodes (Fig. 4B), corrected voltammograms displayed current magnitude almost 350 times larger on Pt-black electrodes. In order to verify that the time-course and concentration level of NO• produced were adequately monitored, the kinetic profile of NO• was also analyzed from series of UV-Vis spectra monitored under the same conditions since their variations tracked the rate of DEA-NONOate decomposition only (Fig. 4D). In this case, an average value of k_1 could be determined at λ = 250 nm with $k_1 = (7.8 \pm 0.5)\,10^{-4}\,s^{-1}$ (Fig. 5A). By introducing this value in Eq. (9), k_2 was evaluated from the best fit of a series of chronoamperometric curves monitored at 0.62 V/REF at several DEA-NONOate concentrations. For that purpose, the diffusion coefficient of NO• was considered to be equal to $1.5\,10^{-5}\,cm^2s^{-1}$ [44] and currents were estimated on the basis of theoretical predictions accounting

for the local hydrodynamic regime [48]. A good agreement was observed between experimental and calculated currents for all initial DEA-NONOate concentration only for $k_2[O_2] = 5.5\,10^2\,M^{-1}s^{-1}$ (Fig. 5B). Since O_2 solubility at room temperature was about 0.27 mM, this afforded $k_2 = (2.2 \pm 0.4)\,10^6\,M^{-2}s^{-1}$. All these results were thus perfectly consistent with values of k_1 and k_2 reported in the literature [46,61–66].

On the basis of these kinetic determinations, a calibration curve was established over a submillimolar concentration range by evaluating NO• concentrations at the time of each chronoamperometric measurement. Accordingly, a linear variation was obtained over two decades (Fig. 5C and D) showing that NO• detection on Pt-black electrodes was very reliable over this concentration range. Note that the upper limit corresponded to the initial concentration of DEA-NONOate that could be used experimentally. Note also that the linear curves reported in these figures did not represent the result of curve fits but were the theoretical line predicted from the previous determined values of k_1 and k_2. The LOD resulting from repetitive measurements at low NO• concentrations (i.e., close to 50 nM) was about 30 nM. This limit was similar to those already reported under various conditions with different geometries and electrode dimensions [25,26,29,40,67–71]. However, the sensitivity reached here was 2.87 $AM^{-1}cm^{-2}$, being higher by one order of magnitude than previously reported ones.

3.3. Detection of ROS and RNS mixtures

Oxidation of $ONOO^-$ at Pt-black electrode occurs at potentials close to H_2O_2 oxidation [44]. A similar situation may apply to NO• oxidation in presence of NO_2^- [45]. In order to be able to perform quantitative analysis of ROS and RNS mixtures at Pt-black electrodes, preliminary tests were thus performed to ensure (i) that no interferences or competitive reactions occurred during simultaneous oxidations and (ii) that the relative contributions of one species to the global response could easily recovered at every detection potential. The choice of an optimal detection potential for one species corresponded to a compromise between reaching a limiting current (i.e., a current plateau) and minimizing the influence of the others ROS/RNS on each individual current response. In the case of simultaneous detections of two species, it was convenient to select a potential related to significant contributions of the species involved.

Voltammetric profiles of H_2O_2 and NO_2^- were thus established separately at pH 7.4 under identical conditions. They are reported and compared in Fig. 6A to those monitored for NO• and $ONOO^-$. Note that $ONOO^-$ profile was recorded at pH 11.1 owing to its chemical stability. It was checked that its electrochemical oxidation (Eq. (4)) was pH independent for conditions approaching physiological ones (data not shown). As observed, oxidation of H_2O_2 overlapped strongly with that of $ONOO^-$ while oxidation profiles of NO• and NO_2^- were well separated from the others. Accordingly, four optimal detection potentials were defined as reported by the vertical dashed lines in Fig. 6A. Note that 0.45 and 0.62 V/REF were potentials selected previously for $ONOO^-$ and NO• detections. Relative influences of H_2O_2 and $ONOO^-$ at 0.3 and 0.45 V/REF were then analyzed from the voltammetric profiles and from current responses obtained from a series of microinjections performed at these potentials (Fig. 6B and C). Owing to the results in Fig. 6A, one had:

$$i = 0.85 i_{H2O2} + 0.43 i_{ONOO-} \text{ at } E = 0.30\,V/REF \quad (11)$$

and:

$$i = i_{H2O2} + i_{ONOO-} \text{ at } E = 0.45\,V/REF \quad (12)$$

where i is the global current measured at each potential. These relations were tested and validated experimentally by comparing

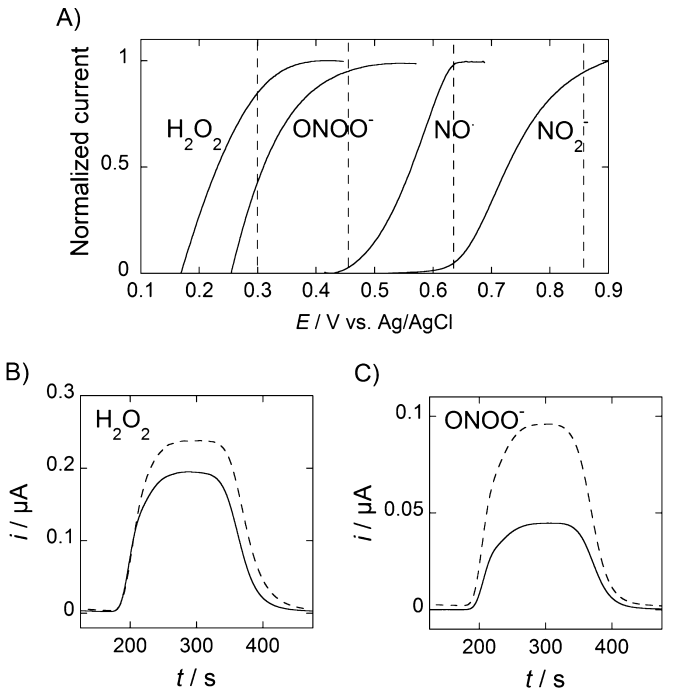

Fig. 6. (A) Normalized steady-state voltammograms obtained at Pt-black electrodes from separate flowing solutions of H_2O_2, $ONOO^-$, NO• and NO_2^-. pH = 7.4 for H_2O_2, NO• and NO_2^- and pH = 11.1 for $ONOO^-$. Dashed lines define the potentials in amperometry offering the best sensitivity and selectivity for the detection of each species. From left to right: E = 0.30, 0.45, 0.62 and 0.85 V/REF. (B) Current responses of 0.1 mM H_2O_2 microinjections at pH = 7.4. E = 0.3 V/REF (solid line) and E = 0.45 V/REF (dashed line). (C) Current responses of 0.1 mM $ONOO^-$ microinjections at pH = 11.1. E = 0.3 V/REF (solid line) and E = 0.45 V/REF (dashed line).

current responses monitored with separate H_2O_2 and $ONOO^-$ solutions and mixtures of identical concentrations. These experiments were conducted at pH 8.4 (at pH slightly higher than physiological conditions) in order to detect enough amount of $ONOO^-$ (see decomposition kinetics in Fig. 2D). This pH value offered a good compromise for testing the performance of the electrochemical detections with synthetic mixtures since it provided the necessary time delay between the solution preparation and measurements. Fig. 7A and B illustrate the perfect agreement obtained between currents in case of microinjections performed at this pH. The sum of individual currents matched the current measured for the corresponding mixture at each potential.

The same approach was applied for detection of the two other species NO• and NO_2^- at 0.62 and 0.85 V/REF. On the basis of the voltammetric profiles reported in Fig. 6A one obtained within the accuracy of the measurements:

$$i = (i_{H2O2} + i_{ONOO-}) + i_{NO} \qquad \text{at } E = 0.62\,V/REF \quad (13)$$

and:

$$i = (i_{H2O2} + i_{ONOO-}) + i_{NO} + i_{NO2-} \qquad \text{at } E = 0.85\,V/REF \quad (14)$$

These relations were also confirmed by series of microinjections performed at these two potentials (Fig. 7C and D). Finally, the good agreement observed between data demonstrated that it was possible at the time scale of these measurements to evaluate the contribution of all the four species and therefore to assess the composition of unknown mixtures of H_2O_2, $ONOO^-$, NO• and NO_2^-. Indeed, provided that the mass transport regime in microchannel is well controlled and predicted [48,72,73], the determination of mixture composition from Eqs. (11) to (14) is straightforward. These results clearly suggested that no side reaction occurred during simultaneous oxidations of the four species. It gives the opportunity to detect, characterize and quantify small amounts of the

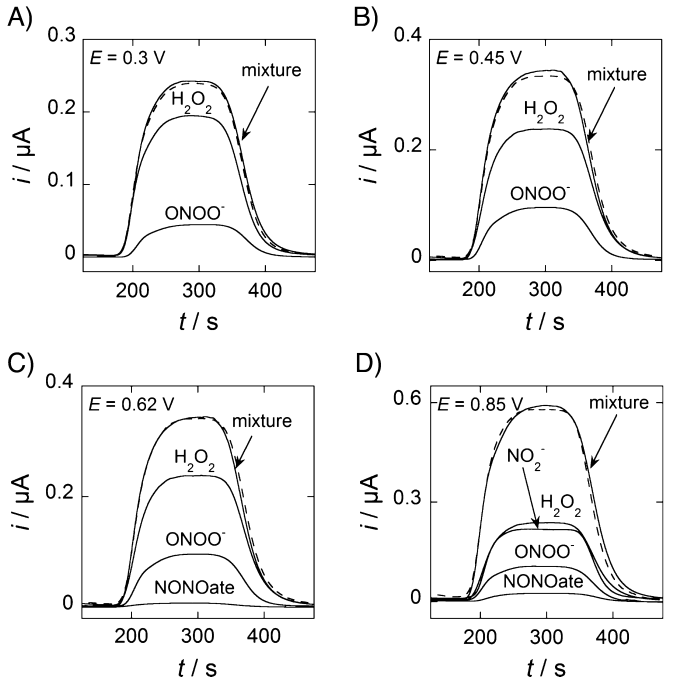

Fig. 7. Current responses at Pt-black electrode as a function of the detection potential with microinjections of 0.1 mM separate solutions and mixtures of H_2O_2, $ONOO^-$, DEA-NONOate and NO_2^- at pH = 8.4. In dashed line, sum of individual current responses obtained from separate solutions.

four ROS/RNS when released by populations of living cells [74]. Note that in such case, the oxidation wave of superoxide anion $O_2^{\bullet-}$ is not expected to produce any interfere in these determinations since $O_2^{\bullet-}$ concentration will be much lower than H_2O_2 due to its fast disproportionation reaction [56] (additionally catalyzed by SOD) or fast reaction with NO• [5]. However, the accuracy of measurements for NO• detection in biological media [42,75] is still a relevant question. Finally, physiological pHs should be leading to correct results whenever ROS/RNS transport between the cells and the detecting electrodes is fast enough. Indeed, under our conditions designed as not to stress the cells hydrodynamically (i.e., at a realistic flow rate of 2 µLmin^{-1} and with a microchannel cross section of 20 × 200 µm), the distance between cells and electrodes needs to be less than 1 cm to ensure a transit time below the second timescale. This is fully consistent with the half life time of peroxynitrite [52], which is the most reactive of the four species.

4. Conclusion

As in the case of H_2O_2 and NO_2^-, electrochemical oxidations of $ONOO^-$ and NO• at optimized Pt-black electrodes led to high detection performances under microfluidic conditions. High reliability and sensitivity of the measurements were achieved allowing kinetic parameters to be determined accurately. Individual detections and quantifications were successfully performed in case of mixtures of the four species. Indeed, upon taking into account the steady-state mass transport regimes achieved at microchannel electrodes, relative composition of solutions could be evaluated at selected detection potentials.

These results validate the concept of simultaneous electrochemical detections of the four important ROS and RNS in microfluidic devices with the use of very small amount of analytes and living biological materials. Temporal resolution below the second-timescale can be easily achieved at channel microelectrodes owing to the geometry of the device and flow velocity. This study opens the way to perform measurements under physiological conditions, in particular to detect locally reactive species like $ONOO^-$ and NO• very close from their production sites. Work is under progress to extend this approach to the detection of oxidative stress metabolites emitted by living cells.

Acknowledgments

This work has been supported in part by the CNRS (UMR8640), Ecole Normale Supérieure, UPMC and French Ministry of Research. Y. L. thanks the China Scholarship Council and the Chinese Embassy for a PhD grant.

References

[1] P. Pacher, J.S. Beckman, L. Liaudet, Phys. Rev. 87 (2007) 315.
[2] V.C. Besson, N. Croci, R.G. Boulu, M. Plotkine, C. Marchand-Verrecchia, Brain. Research. 989 (2003) 58.
[3] C. Amatore, S. Arbault, M. Guille, F. Lemaître, Chem. Rev. 108 (2008) 2585.
[4] J.C. Toledo Jr., O. Augusto, Chem. Res. Toxicol. 25 (2012) 975.
[5] R. Kissner, T. Nauser, P. Bugnon, P.G. Lye, W.H. Koppenol, Chem. Res. Toxicol. 10 (1997) 1285.
[6] D. Jourd'heuil, F.L. Jourd'heuil, P.S. Kutchukian, R.A. Musah, D.A. Wink, M.B. Grisham, J. Biol. Chem. 276 (2001) 28799.
[7] M.K. Hulvey, C.N. Frankenfeld, S.M. Lunte, Anal. Chem. 82 (2010) 1608.
[8] D. Quinton, S. Griveau, F. Bedioui, Electrochem. Commun. 12 (2010) 1446.
[9] O.C. Zafiriou, M. McFarland, Anal. Chem. 52 (1980) 1662.
[10] J.N. Bates, Neuroprotocols 1 (1992) 141.
[11] D.C. Yao, A.G. Vlessidis, N.P. Evmiridis, A. Evangelou, S. Karkabounas, S. Tsampalas, Anal. Chim. Acta 458 (2002) 281.
[12] M.M. Tarpey, D.A. Wink, M.B. Grisham, Am. J. Physiol. Regul. Integr. Comp. Physiol. 286 (2004) R431.
[13] P. Wardman, Free Radic. Biol. Med. 43 (2007) 995.
[14] Y.Y. Woldman, J. Sun, J.L. Zweier, V.V. Khramtsov, Free Radic. Biol. Med. 47 (2009) 1339.
[15] T. Nagano, J. Clin. Biochem. Nutr. 45 (2009) 111.
[16] R. Radi, T.P. Cosgrove, J.S. Beckman, B.A. Freeman, Biochem. J. 290 (1993) 51.
[17] C.C. Winterbourn, Biochim. Biophys. Acta 1840 (2014) 730.
[18] R.M. Wightman, Science 311 (2006) 1570.
[19] Y. Wang, J.M. Noel, J. Velmurugan, W. Nogala, M.V. Mirkin, C. Lu, M. Guille Collignon, F. Lemaitre, C. Amatore, Proc. Natl. Acad. Sci. USA 109 (2012) 11534.
[20] S. Borgmann, I. Radtke, T. Erichsen, A. Blochl, R. Heumann, W. Schuhmann, *ChemBioChem* 7 (2006) 662.
[21] S. Isik, J. Castillo, A. Blochl, E. Csoregi, W. Schuhmann, Bioelectrochemistry 70 (2007) 173.
[22] V.L. Lobachev, E.S. Rudakov, Uspekhi Khimii 75 (2006) 422.
[23] S. Borgmann, Anal. Bioanal. Chem. 394 (2009) 95.
[24] D. Gupta, B. Harish, R. Kissner, W.H. Koppenol, Dalton Trans. (2009) 5730.
[25] F. Bedioui, D. Quinton, S. Griveau, T. Nyokong, Phys. Chem. Chem. Phys. 12 (2010) 9976.
[26] B.J. Privett, J.H. Shin, M.H. Schoenfisch, Chem. Soc. Rev. 39 (2010) 1925.
[27] D.B. Gunasekara, M.K. Hulvey, S.M. Lunte, Electrophoresis 32 (2011) 832.
[28] D.B. Gunasekara, M.K. Hulvey, S.M. Lunte, J.A. da Silva, Anal. Bioanal. Chem. 403 (2012) 2377.
[29] R.A. Hunter, B.J. Privett, W.H. Henley, E.R. Breed, Z. Liang, R. Mittal, B.P. Yoseph, J.E. McDunn, E.M. Burd, C.M. Coopersmith, J.M. Ramsey, M.H. Schoenfisch, Anal. Chem. 85 (2013) 6066.
[30] C. Amatore, S. Arbault, D. Bruce, P. de Oliveira, M. Erard, M. Vuillaume, Chem. Eur. J. 7 (2001) 4171.
[31] G. Ferrer-Sueta, R. Radi, ACS Chem. Bio. 4 (2009) 161.
[32] O. Adegoke, T. Nyokong, J. Lumin. 134 (2013) 448.
[33] S. Arbault, N. Sojic, D. Bruce, C. Amatore, A. Sarasin, M. Vuillaume, Carcinogenesis 25 (2004) 509.
[34] C. Amatore, S. Arbault, C. Bouton, K. Coffi, J.-C. Drapier, H. Ghandour, Y. Tong, ChemBioChem 7 (2006) 653.
[35] C. Amatore, S. Arbault, M. Erard, Anal. Chem. 80 (2008) 9635.
[36] C. Amatore, S. Arbault, Y. Chen, C. Crozatier, I. Tapsoba, Lab Chip 7 (2007) 233.
[37] C. Amatore, S. Arbault, C. Bouton, J.-C. Drapier, H. Ghandour, A.C.W. Koh, ChemBioChem 9 (2008) 1472.
[38] M.R. Filipovic, A.C.W. Koh, S. Arbault, V. Niketic, A. Debus, U. Schleicher, C. Bogdan, M. Guille, F. Lemaitre, C. Amatore, I. Ivanovic-Burmazovic, Angew. Chem. Int. Edit. 49 (2010) 4228.
[39] A.S. Bernard, C. Giroud, H.Y. Ching, A. Meunier, V. Ambike, C. Amatore, M. Guille Collignon, F. Lemaitre, C. Policar, Dalton Trans. 41 (2012) 6399.
[40] W. Cha, Y.-C. Tung, M.E. Meyerhoff, S. Takayama, Anal. Chem. 82 (2010) 3300.
[41] E.C. Metto, K. Evans, P. Barney, A.H. Culbertson, D.B. Gunasekara, G. Caruso, M.K. Hulvey, J.A. Fracassi da Silva, S.M. Lunte, C.T. Culbertson, Anal. Chem. 85 (2013) 10188.
[42] J.L. Harding, M.M. Reynolds, Anal. Chem. 86 (2014) 2025.
[43] M.W. Breiter, Electrochim. Acta 11 (1966) 905.
[44] Y. Li, C. Sella, F. Lemaitre, M.G. Collignon, L. Thouin, C. Amatore, Electroanalysis 25 (2013) 895.

[45] C. Amatore, S. Arbault, Y. Bouret, B. Cauli, M. Guille, A. Rancillac, J. Rossier, ChemPhysChem 7 (2006) 181.
[46] S. Griveau, C. Dumezy, P. Goldner, F. Bedioui, Electrochem. Commun. 9 (2007) 2551.
[47] Y. Ikariyama, S. Yamauchi, T. Yukiashi, H. Ushioda, J. Electrochem. Soc. 136 (1989) 702.
[48] C. Amatore, N. Da Mota, C. Sella, L. Thouin, Anal. Chem. 79 (2007) 8502.
[49] W.H. Koppenol, Quimica Nova 21 (1998) 326.
[50] Y. Luo, C. Zhang, Y. She, R. Zhong, P. Wei, Reac. Kinet. Mech. Cat. 101 (2010) 291.
[51] S. Pfeiffer, A.C.F. Gorren, K. Schmidt, E.R. Werner, B. Hansert, D.S. Bohle, B. Mayer, J. Biol. Chem. 272 (1997) 3465.
[52] C. Molina, R. Kissner, W.H. Koppenol, Dalton Trans. 42 (2013) 9898.
[53] S. Tibi, W.H. Koppenol, Helv. Chim. Acta 83 (2000) 2412.
[54] J.P. Crow, Free Radic. Biol. Med. 28 (2000) 1487.
[55] Z.J. Chen, W. Ren, Q.E. Wright, H.W. Ai, J. Am. Chem. Soc. 135 (2013) 14940.
[56] B.H.J. Bielski, D.E. Cabelli, R.L. Arudi, J. Phys. Chem. Ref. Data 14 (1985) 1041.
[57] R.B. Mikkelsen, P. Wardman, Oncogene 22 (2003) 5734.
[58] I.G. Zacharia, W.M. Deen, Ann. Biomed. Eng. 33 (2005) 214.
[59] X. Liu, J.L. Zweier, J. Electroanal. Chem. 688 (2013) 32.
[60] L.K. Keefer, R.W. Nims, K.M. Davies, D.A. Wink, Methods Enzymol. 268 (1996) 281.
[61] J.A. Hrabie, J.R. Klose, D.A. Wink, L.K. Keefer, J. Org. Chem. 58 (1993) 1472.
[62] V.L. Pogrebnaya, A.P. Usov, A.V. Baranov, A.I. Nesterenko, P.I. Bezyazychnyi, J. App. Chem. Ussr 48 (1975) 1004.
[63] V.G. Kahritonov, A.R. Sundquist, V.S. Sharma, J. Biol. Chem. 269 (1994) 5881.
[64] R.S. Lewis, W.M. Deen, Chem. Res. Toxicol. 7 (1994) 568.
[65] M. Pires, M. Rossi, D. Ross, Int. J. Chem. Kin. 26 (1994) 1207.
[66] S. Goldstein, G. Czapski, J. Am. Chem. Soc. 117 (1995) 12078.
[67] A. Cserey, M. Gratzl, Anal. Chem. 73 (2001) 3965.
[68] F. Bedioui, N. Villeneuve, Electroanalysis 15 (2003) 5.
[69] I.R. Davies, X. Zhang, Methods Enzymol. 436 (2008) 63.
[70] D. Quinton, A. Girard, L.T.T. Kim, V. Raimbault, L. Griscom, F. Razan, S. Griveau, F. Bedioui, Lab Chip 11 (2011) 1342.
[71] S. Griveau, F. Bedioui, Anal. Bioanal. Chem. 405 (2013) 3475.
[72] C. Amatore, N. Da Mota, C. Sella, L. Thouin, Anal. Chem. 80 (2008) 4976.
[73] C. Amatore, C. Lemmer, P. Perrodin, C. Sella, L. Thouin, Electrochem. Commun. 13 (2011) 1459.
[74] C. Amatore, S. Arbault, A.C.W. Koh, Anal. Chem. 82 (2010) 1411.
[75] R.A. Hunter, W.L. Storm, P.N. Coneski, M.H. Schoenfisch, Anal. Chem. 85 (2013) 1957.